Journal of Computational Electronics 2: 123–126, 2003

"Atomistic", Quantum and Ballistic Effects in Nanoscale MOSFETs

G. FIORI AND G. IANNACCONE
Dipartimento di Ingegneria dell'Informazione, Università degli studi di Pisa, Via Diotisalvi 2, I-56122, Pisa, Italy
g.fiori@iet.unipi.it
g.iannaccone@iet.unipi.it

Abstract. In this paper we describe the effects of quantum confinement and ballistic transport in the channel on the dispersion of threshold voltage due to the discrete distribution of dopants. To this aim, a recently developed 3D Poisson-Schrödinger solver is used, along with a 2D solver of ballistic transport. The Schrödinger equation is solved with density functional theory, in the local density approximation. Results on statistically meaningful ensembles of devices show that both ballistic transport and quantum confinement lead to an increase of threshold voltage dispersion.

Keywords: MOSFETs, atomistic effects, quantum modeling, ballistic transport

1. Introduction

CMOS feature sizes have by now reached the sub-100 nm regime, and in the 2007 25 nm channel length transistors are going to be produced, as foreseen by the ITRS'01. In this perspective, from a design point of view, a modern device simulator needs to address typical aspects of nanoscale transport: "atomistic" distribution of dopants, quantum confinement of carriers and far from equilibrium transport in the channel.

In MOSFET devices of the latest technology node, the number of impurities in the depletion region is of the order of hundreds, therefore intrinsic fluctuations of the number and of the position of impurities strongly influence the value of the threshold voltage. This has been proven experimentally in a pioneering work by Mizuno [1], and investigated from the theoretical point of view by means of simulations [2–4], and by analytical models [5–8]. On the other hand, a quantitatively accurate investigation of the threshold voltage dispersion requires the use of quantum models, in order to take into account the threshold voltage shift due to the increased confinement of electrons in the channel [6,9].

Moreover, already in 0.13 μm MOSFETs, a significant fraction of electrons traverse the channel without energy loss and with conservation of transversal momentum [10]. In this perspective, accurate simulations need to consider the ballistic fraction of electrons contributing to transport.

We have developed a three dimensional Poisson-Schrödinger solver based on density functional theory, with local density approximation. This code allows us to study all the above mentioned effects. In particular we focus our attention on a 50 nm MOSFET with uniform doping in the bulk, for which comparable data on threshold voltage dispersion, based on semiclassical models or on density gradient approximations, are available [3,4].

2. Results

We have solved the self-consistent Poisson-Schrödinger equation in the three-dimensional domain in order to take into account quantum confinement of electrons in the channel. Because quantum confinement is predominant along the direction perpendicular to the Si/SiO_2 interface (x axis), we have decoupled the Schrödinger equation into two parts, one along the x axis and one in the y-z plane: discrete energy levels appear along x, while a semiclassical expression correctly approximates the in-plane states because of the negligible confinement. In this way

an excessive computational burden is avoided, introducing only a negligible error [11]. The equations have been discretized by means of the box-integration method over a rectangular grid and the nonlinear system has been solved iteratively with the Newton-Raphson method with the predictor/corrector approach described in [12].

The simulated structure is a n-MOSFET with channel length of 50 nm, gate oxide thickness of 3 nm and doping concentration $N_A = 5 \times 10^{18}$ cm^{-3}.

First, we need to adopt a definition of threshold voltage. In particular, we define the threshold voltage as the intercept with the voltage axis of the line that provides the best fit of the transfer characteristics at low V_{DS} in the strong inversion region.

Such characteristics are computed in the limit of fully ballistic transport, with a model widely explained in our previous work [13], and in the case of drift-diffusion transport, from the conductance obtained by solving a simplified continuity equation [3]. In 50 nm devices a significant fraction of electrons traverse the channel without energy loss, so the transport regime should be intermediate between the two considered cases.

Both approaches, however, are too computationally demanding to be used in statistical simulations, therefore we use a simplified method, consisting in extracting V_T from the intercept of the fitting line of the curve representing the charge integrated in a region in the channel as a function of V_G.

Figure 1 show the threshold voltage computed by means of the ballistic and the simplified drift/diffusion model (straight lines) and the threshold voltage obtained computing the charge in the channel (diamonds) as a function of the width of the region of integration in the channel direction. As it can be noticed, the length of the intervals centered in the middle of the channel equal to 26 nm and 40 nm fit well the ballistic and the quasi-equilibrium threshold voltage, respectively. Indeed, in case of the ballistic model, only the carriers very close to the maximum of the subband contribute to the current, while in the drift/diffusion model, all regions of the channel contribute equally to channel conductance.

The above described threshold voltage extraction procedure has been used to compute the threshold voltage statistics, performing simulations over 100 devices with the same nominal doping profile, but with different atomistic distribution. The random dopant profile has been generated by assuming a Poisson distribution with average equal to the number of atoms in the Voronoi cell. Moreover, in order to obtain a random dopant distribution with at most one dopant atom contained in each cell, we have chosen a grid with a maximum spacing of 1 nm.

Figure 2 shows the quantum and semiclassical threshold voltage standard deviation as a function of the doping concentration in the bulk, in the quasi-equilibrium case. As expected, the standard deviation computed semiclassically (σ_{sc}) is smaller than that computed by means of quantum models (σ_Q), since the threshold voltage standard deviation is a rising monotonic function of the oxide thickness, which is effectively increased by quantum confinement. For the same reason, we can notice that the two curves are almost shifted. Indeed, as the carrier centroid along the

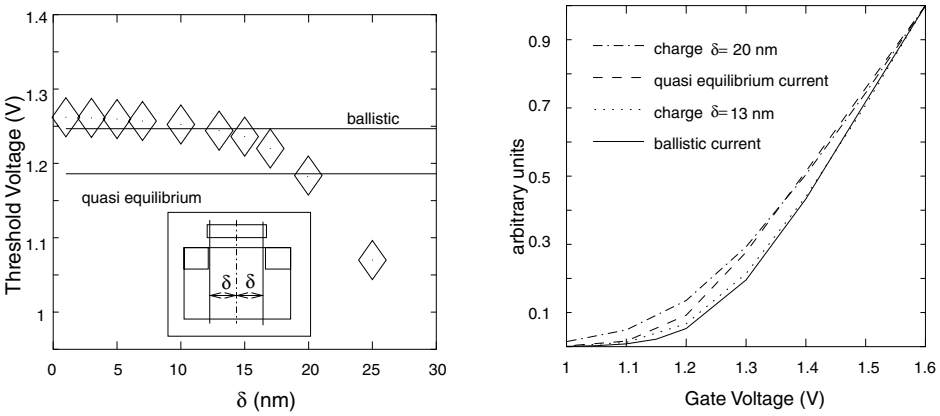

Figure 1. Threshold voltage extracted by the charge plot computed in a region of dimension $50 \times 50 \times \delta$ nm^3, by ballistic and simplified drift/diffusion models (left). Comparison between charge in region $50 \times 50 \times \delta$ nm^3 and quasi equilibrium or ballistic current (right).

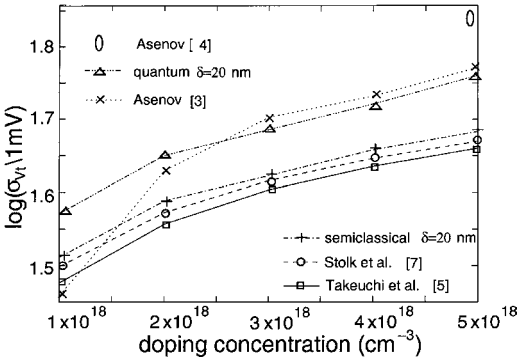

Figure 2. Semiclassical and quantum standard deviation computed with the simplified drift/diffusion model as a function of the doping concentration. Standard deviation computed in [3–5] and in [7] are also shown.

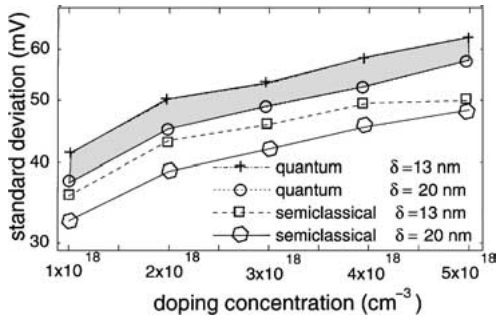

Figure 3. Semiclassical and quantum threshold voltage standard deviation computed with the simplified drift/diffusion and ballistic model.

vertical direction varies in the range of $1 \div 1.3$ nm as the doping factor is varied, the percentage increase of the oxide thickness is about 13.5%, that in the semilog plot corresponds to a shift of approximately 55×10^{-2}.

In Fig. 2 are also shown semiclassical and quantum results obtained in [3,4] and those derived by the analytical model described in [5,7]. As can be noticed, our results differ from results in [3,4], and this is probably due to the different definition of threshold voltage. Indeed, while in our case the threshold voltage is defined in deep inversion, in the case of [3] the threshold voltage is defined as the gate voltage at which the source-to-drain current is equal to 10^{-8} A, i.e., in weak inversion or in subthreshold conditions, where random percolating paths may have a role in increasing the dispersion of threshold voltage.

Semiclassical simulations are instead in very good agreement with the analytical expression based on a simple 1D model [7], since the dispersion of V_T depends in practice only on the vertical distribution of dopants and also because in the considered devices charge sharing effects are negligible: indeed, simulations performed on a MOS structure with the same doping yield a threshold voltage that differs from that of the MOSFET only by 30 mV.

In Fig. 3 the standard deviation is plotted as a function of doping, in case of ballistic and quasi-equilibrium simulations of threshold voltage. In this way it is possible to define an upper and a lower limit for the standard deviation of V_T, depending on the degree of ballistic transport. In particular, considering quantum effects, the device should belong to the highlighted region of Fig. 3.

From simulations it has also been possible to obtain an interesting relation between the random variables V_{TQ} and V_{Tsc}, i.e., the threshold voltages computed with quantum and semiclassical models, respectively. In particular, the two random variables are strictly correlated (the correlation factor is always larger than 0.997 for all simulated devices), and a linear relation can be found for them: $V_{\mathrm{TQ}} = mV_{\mathrm{Tsc}} + q$ (Fig. 4).

In Table 1 the best fitting values of m are compared with the ratio $\frac{\sigma_Q}{Q_{\mathrm{sc}}}$ for both the ballistic and the quasi equilibrium case, and are practically identical, suggesting that charge centroid and quantum capacitance are responsible for the difference between σ_Q and σ_{sc}.

Since results derived from analytical formulae and semiclassical simulations are in good agreement, and since quantum and semiclassical threshold voltages are linearly dependent, in case of reduced charge sharing effects, the above shown results suggest a simple way to correct the semiclassical expression for the threshold voltage dispersion, in order to include quantum effects.

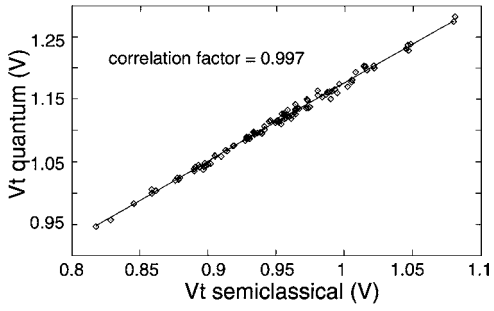

Figure 4. Scatter plot of the threshold voltage computed by means of quantum model versus semiclassical threshold voltage.

Table 1. Ratio between quantum and semiclassical standard deviation of the threshold voltage (σ_Q and σ_{sc}, respectively) derived from simulations and from the scatter plot.

	Ballistic		Quasi equilibrium	
Doping factor	m	$\frac{\sigma_Q}{\sigma_{sc}}$	m	$\frac{\sigma_Q}{\sigma_{sc}}$
1.0	1.253	1.256	1.196	1.196
0.8	1.18	1.183	1.163	1.164
0.6	1.159	1.16	1.164	1.166
0.4	1.158	1.16	1.162	1.172
0.2	1.16	1.162	1.172	1.146

3. Conclusion

We have developed a three-dimensional Poisson-Schrödinger solver that takes into account at the same time the effects of the discrete distribution of dopants and of the quantum confinement in the channel on the threshold voltage.

The threshold voltage standard deviation computed by means of quantum models is larger than that computed semiclassically, due to the increase of the effective oxide thickness.

Moreover, performed simulations have shown that also ballistic transport in the channel increases the dispersion of the threshold voltage. In particular, fluctuations of V_T in the case of ballistic transport depend on fluctuations of the subband maximum, that are mainly due to fluctuations of the impurity number in a small volume in the central region of the device (at small drain voltage).

Quantum confinement has on the standard deviation of V_T an effect that is shown to be strongly correlated to that on V_T, and is basically due to the inversion layer capacitance.

References

1. T. Mizuno, J. Okamura, and A. Toriumi, *IEEE Trans. Electron Devices*, **41**, 2116 (1994).
2. H.S. Wong and Y. Taur, *Proc. IEDM 1993. Dig. Tech.*, 705 (1993).
3. A. Asenov, *IEEE Trans. Electron Devices*, **45**, 2505 (1998).
4. A. Asenov, G. Slavcheva, A.R. Brown, J.H. Davies, and S. Saini, *IEEE Trans. Electron Devices*, **48**, 722 (2001).
5. K. Takeuchi, T. Tatsumi, and A. Furukawa, *IEDM Tech. Digest*, 841 (1997).
6. Y. Taur and T.H. Ning, *Fundamentals of Modern VLSI Devices* (Cambridge University Press, Cambridge UK, 1998), pp. 194–202.
7. P.A. Stolk, F.P. Widdershoven, and D.B.M. Klaassen, *IEEE Trans. Electron Devices*, **45**, 1960 (1998).
8. K.R. Lakshmikumar, R.A. Hadaway, and M.A. Copeland, *IEEE Journal of Solid-State Circuits*, **21**, 1057 (1986).
9. Y. Taur, D.A. Buchanan, W. Chen, D.J. Frank, K.E. Ismail, S.H. Lo, G.A. Sail-Lalasz, R.G. Viswanathan, H.J.C. Wann, S.J. Wind, and H.S. Wong, *Proc. IEEE*, **85**, 486 (1997).
10. Z. Ren, R. Venugopal, S. Datta, and M. Lundstrom, *IEDM Tech. Dig.*, 715 (2000).
11. G. Fiori and G. Iannaccone, *Nanotechnology*, **13**, 294 (2002).
12. A. Trellakis, A.T. Galick, A. Pacelli, and U. Ravaioli, *J. Appl. Phys.*, **81**, 7800 (1997).
13. G. Fiori and G. Iannaccone, *Appl. Phs. Lett*., **81**, 19 (2002).